J. Kor. Powd. Met. Inst., Vol. 20, No. 3, 2013
DOI: 10.4150/KPMI.2013.20.3.221

Fabrication of Fe-TiB_2 Composite Powder by High-Energy Milling and Subsequent Reaction Synthesis

H. X. Khoa, N. Q. Tuan, Y. H. Lee, B. H. Lee, N. H. Viet[a], and J. S. Kim*

School of Materials Science and Engineering, University of Ulsan, San-29, Mugeo-2 Dong, Nam-Gu, Ulsan, 680-749, Korea

[a]School of Materials Science and Engineering, Hanoi University of Science and Technology, No 1, Dai Co Viet Street, Hai Ba Trung dist, Hanoi, Vietnam

(Received June 11, 2013; Accepted June 24, 2013)

Abstract TiB_2-reinforced iron matrix composite (Fe-TiB_2) powder was in-situ fabricated from titanium hydride (TiH_2) and iron boride (FeB) powders by the mechanical activation and a subsequent reaction. Phase formation of the composite powder was identified by X-ray diffraction (XRD). The morphology and phase composition were observed and measured by field emission-scanning electron microscopy (FE-SEM) and energy-dispersive X-ray spectroscopy (EDS), respectively. The results showed that TiB_2 particles formed in nanoscale were uniformly distributed in Fe matrix. Fe_2B phase existed due to an incomplete reaction of Ti and FeB. Effect of milling process and synthesis temperature on the formation of composite were discussed.

Keywords: Fe-TiB_2 composite, Mechanical activation, Solid state reaction, Heat treatment

1. Introduction

Fe-based metal matrix composites have found many applications in tools, dies and wear-resistant parts for last several decades. Adding refractory particles to the Fe matrix as dispersoid improves mechanical properties of the matrix and increases wear property [1-2]. Among various ceramic particulates, TiB_2 is considered to be one of the best reinforcements for steel matrix due to its high melting point (2980°C), high hardness (3400 kg/mm^2, only lower than diamond, BN and B_4C), high elastic modulus, good corrosion resistance and chemical inertness. In terms of thermal and electrical conductivities, TiB_2 is favoured in selection because of its high thermal (60-120 W/mK) and electrical (~10^5 S/cm) conductivities.

One of the most common techniques of producing these types of particulate-reinforced metal-matrix composites is powder metallurgy. An important factor influencing the structure and properties of the composites is the ceramic metal interface [2]. Recently, *in situ* technique has been developed to incorporate ceramic particulates into metal matrices. The major advantage of *in situ* process is that the dispersed ceramic phase is created by the chemical reaction between elements of their compounds so that the particles are formed within the metal matrix and are clean, non-oxidized particle-matrix interfaces with higher interfacial strength, improved wettability and better particle-size distribution [3]. The synthesis of TiB_2 phase by various methods have been given: laser cladding [4-5], plasma transferred arc (PTA) [6], aluminothermic reduction [7], and self-propagating high temperature synthesis (SHS) [2, 8]. They indicate that TiB_2 particles are able to form in situ via different routes from various initial materials. Some of them used pure elements as starting materials which is costly unfavourable. Most of them exhibited large TiB_2 particle size.

The present work aimed at investigating the feasibility of fabricating TiB_2-reinforced Fe matrix composite powder by a combination of mechanical activation and heat treatment. It is expected that the route is able to provide a novel process for rapid, simple and cost-effective synthe-

*Corresponding Author : Ji Soon Kim, **TEL:** +82-52-259-2244, **FAX:** +82-52-259-1688, **E-mail:** jskim@ulsan.ac.kr

sis method, because of its effective dispersion of the fine reinforcing particles, for Fe-TiB_2 composite using titanium hydride (TiH_2) and ferro-boron (FeB) as initial materials. Effect of milling process and heat treatment on the phase formation of composite powder was included in this study.

2. Experimental

Commercial ferro-boron alloy, FeB, and titanium hydride, TiH_2, powders were used as starting materials. The TiH_2 and FeB powder mixture was accurately weighed in the ratio of 27.2 wt% TiH_2 and 72.8 wt% FeB to give a Fe-38.4wt% TiB_2 composite powder corresponding to the following reaction equation:

$$2FeB_{(s)} + TiH_{2(s)} \rightarrow 2Fe_{(s)} + TiB_{2(s)} + H_{2(g)} \uparrow \quad (1)$$

FeB in a form of lump was manually crushed and screened to remove the large fragment of FeB. The powder mixtures were prepared either by turbular mixing for 2h or by high-energy milling for 2 h in a high-energy ball mill (AGO-2, [9]). Stainless steel vials and balls (5 mm in diameter) were used. The balls-to-powder weight ratio was 20:1. The vials were evacuated and filled with 0.3 MPa pure argon gas before each run to prevent oxidation during processing. The rotational velocity of mill axis was 500 rpm.

To fabricate Fe-TiB_2 composite powders, the reaction of TiH_2 and FeB was carried out in a tube furnace at 1200°C in flowing Ar gas with heating rate of 5°C/min and holding time of 1 and 5 hours.

Particle size was measured using laser scattering particle size analyser, Mastersizer 2000 (Malvern). Phase formation of powder was identified by X-ray diffractometer using Cu K_α radiation. The microstructure and chemical elements of the composite powders were observed and analyzed by field emission scanning electron microscope (FE-SEM) equipped with energy dispersive spectroscopy (EDS).

3. Results and Discussion

3.1. Powder characteristics

The morphology of the starting powders is shown in Fig. 1. Table 1 shows a summary of the particle size analysis. The mean particle size (D_{50}) of TiH_2 and FeB are 12.5 and 7.0 μm, respectively.

Fig. 3 shows morphology of the FeB-TiH_2 powder mixture after high-energy milling (a-b) and its cross-section(c). TiH_2 and FeB are brittle materials, so these powders get fractured easily during milling and their particle size is reduced significantly. Particle size analysis in the D_{10} and D_{50} terms are 1.2 and 3.0 μm respectively. These values prove that the FeB and TiH_2 powder became finer after 2h of high-energy milling in comparison with the starting powders. But the D_{90} value increased after milling process (D_{90} = 23.5 μm) by formation of agglomerates as shown in Fig. 3(a). The image taken on the surface of agglomerate (Fig. 3(b)) shows fine and rounded particles of

Table 1. Result of particle size analysis of starting powders (volume distribution)

Powder	D_{10} (μm)	D_{50} (μm)	D_{90} (μm)	Specific Area (m^2/g)
TiH_2	3.3	12.5	38.6	0.80
FeB	3.1	7.0	16.8	1.05

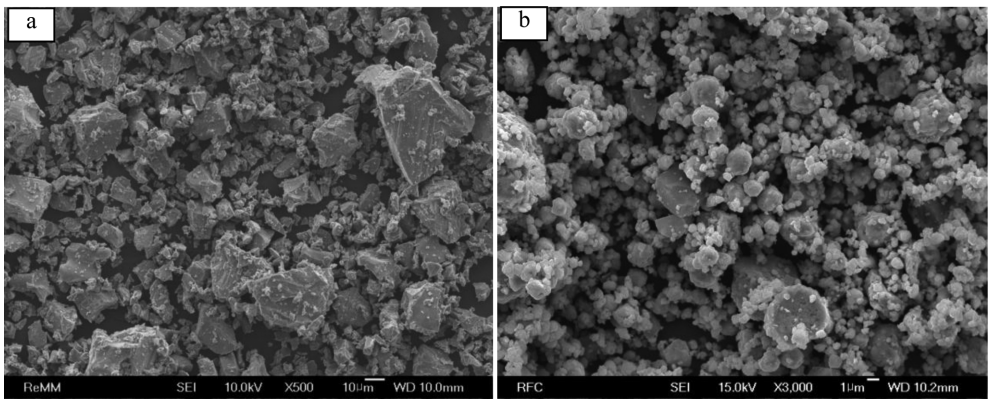

Fig. 1. FE-SEM images of starting powders; (a) TiH_2 and (b) FeB powder.

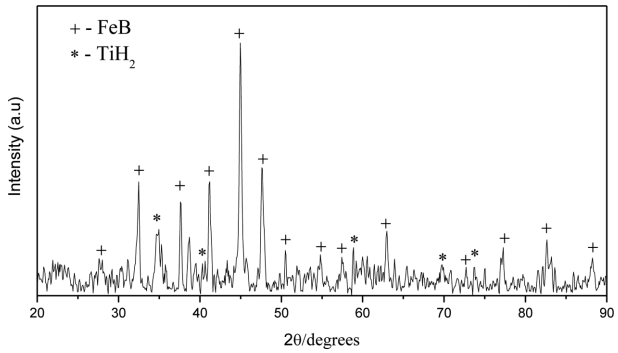

Fig. 2. XRD pattern of the FeB-TiH_2 powder mixture prepared by high-energy milling.

FeB and TiH_2. To observe the agglomerates more clearly, the cross-section of agglomerate was investigated (Fig. 3(c)). Agglomerates formed a dense structure; the TiH_2 (dark phase) homogeneously distributed around the FeB particles. TiH_2 is brittle and can be milled to nanoscale by high-energy milling for short periods of time [10]. The more brittle component TiH_2 gets more easily fragmented and embedded around the less brittle component FeB. After 2h high-energy milling, the FeB particle size decreased and distributed in a broad range from nanometer to several micrometer.

EDS line scan (Fig. 3(d)) on the particle outlines showed the distribution of Fe, Ti and B. The gradual change of Fe and Ti indicates the close contact between FeB and TiH_2.

3.2. Thermal activation of powder mixtures

Fig. 4 shows DSC curve obtained under a constant heating rate of 10 $Kmin^{-1}$ for the FeB-TiH_2 powder mixture prepared by turbular mixing and high-energy milling, respectively. DSC curve for tubular mixing shows two thermal events represented by the first two peaks at 470°C and 520°C assigning for endothermic nature of the dehydrogenation process of TiH_2 compound [10], while the only a peak appeared at 370°C for the high-energy milling powder mixture. The shift to lower temperature for dehydrogenation events can be explained by effect of milling that decreases particle size [10]. At higher temperature, beginning at 1030°C for turbular mixing and 910°C for high-energy milling powder mixtures, respec-

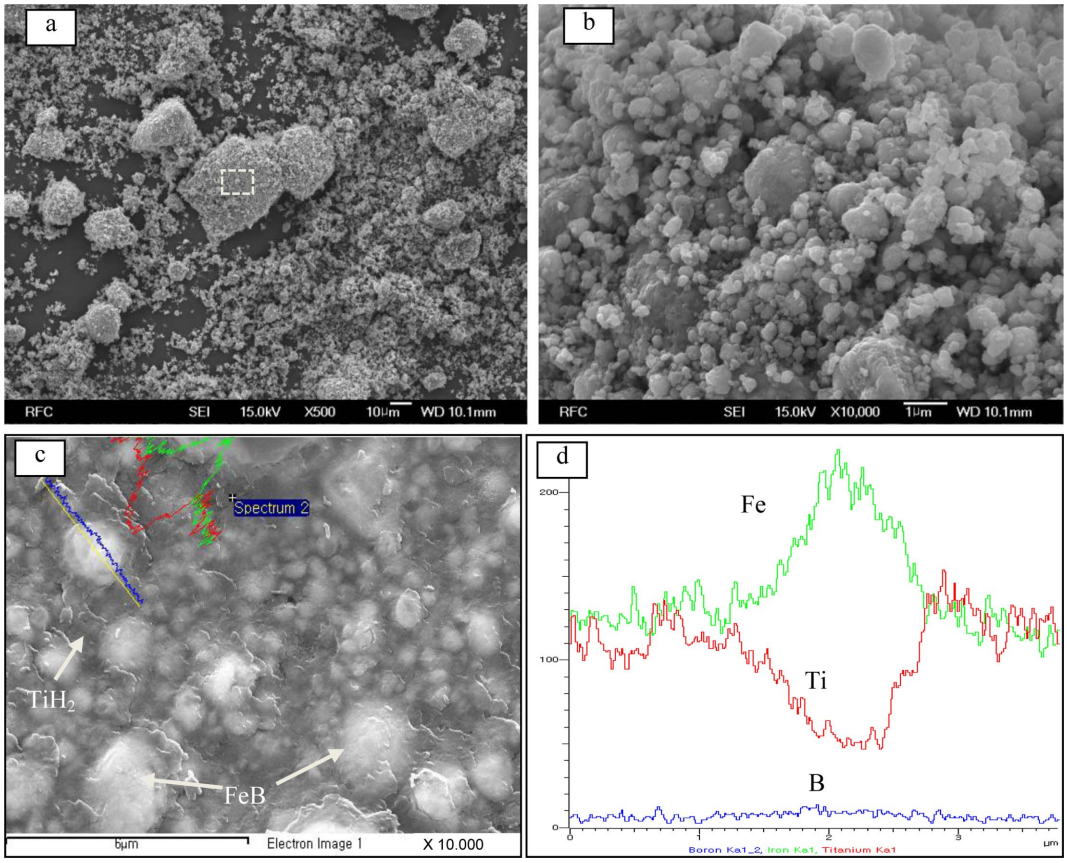

Fig. 3. (a) Fe-SEM image of FeB-TiH_2 powder mixture after high-energy milling for 2h at 500 rpm, (b) the selected area with high magnification, (c) the polished cross-section, and (d) the result of EDS line scan across the particle in (c).

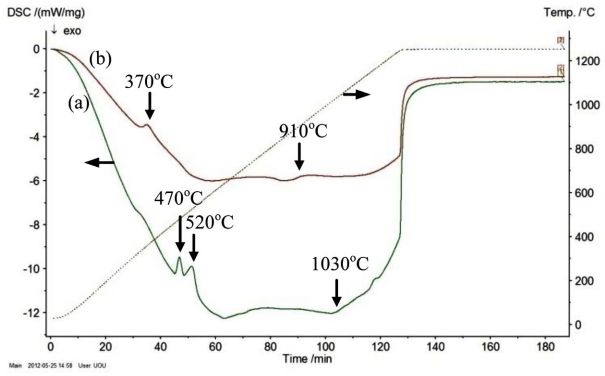

Fig. 4. DSC curves of FeB-TiH_2 powder mixture after (a) 2h turbular mixing and (b) high-energy milling at 500 rpm for 2h (b).

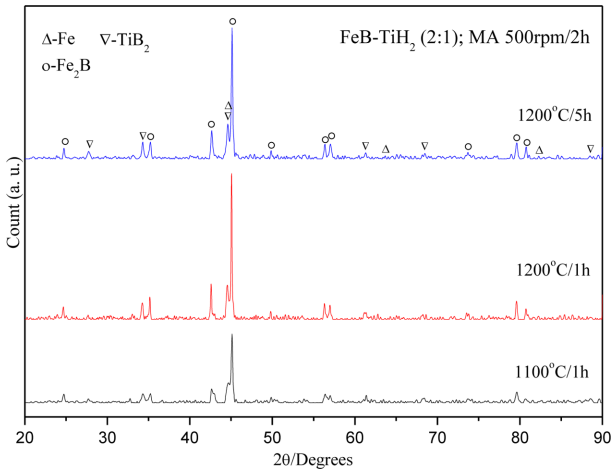

Fig. 5. XRD patterns of high-energy milled powder mixture after synthesis reaction at given conditions of temperature and time.

tively, the DSC curves shifted up signaling for appearing of thermal events. These events can be chemical solid reaction between Ti formed from the dehydrogenation process of TiH_2 with boron in FeB to form TiB_2 phase.

3.3. Phase composition and microstructure of FeB-TiH_2 powder mixture after heat treatment

Fig. 5 shows the XRD patterns of the Fe-TiB_2 composite powders by *in situ* synthesis from FeB-TiH_2 powder mixture. The identified peaks are assigned to Fe, Fe_2B and TiB_2, respectively. There is a clear split of the peak around 45 when increasing temperature of 1100°C to 1200°C.

The possible solid state reactions involved in synthesizing Fe-TiB_2 composite powder has been considered. The reactions leading to formation of Fe-TiB_2 composite can be suggested as follows [11-14]:

$$TiH_2 \rightarrow Ti + H_2\uparrow \quad (2)$$

$$Ti + 4FeB \rightarrow TiB_2 + 2Fe_2B \quad (3)$$

$$Ti + 2Fe_2B \rightarrow TiB_2 + 4Fe \quad (4)$$

The overall reaction of these is reaction (1) presented above. FeB phase was not found but Fe_2B phase exists within the resolution of the XRD pattern. This means the reaction (4) was not completely finished, the remained Fe_2B phase was also reported in [4-7]. During the process, TiH_2 and FeB might interact to form some possible compounds such as TiB_2, TiB or Fe_2B, etc. The Gibbs free energies of formation for these compounds are [2, 14]:

$$Ti + 2B \rightarrow TiB_2 \qquad \Delta G_{1300K} = -275.5\ kJ.mol^{-1} \quad (6)$$

$$2Fe + B \rightarrow Fe_2B \qquad \Delta G_{1300K} = -67.2\ kJ.mol^{-1} \quad (7)$$

$$Ti + B \rightarrow TiB \qquad \Delta G_{1300K} = -155.3\ kJ.mol^{-1} \quad (8)$$

$$Fe + Ti \rightarrow FeTi \qquad \Delta G_{1450K} = -31.0\ kJ.mol^{-1} \quad (9)$$

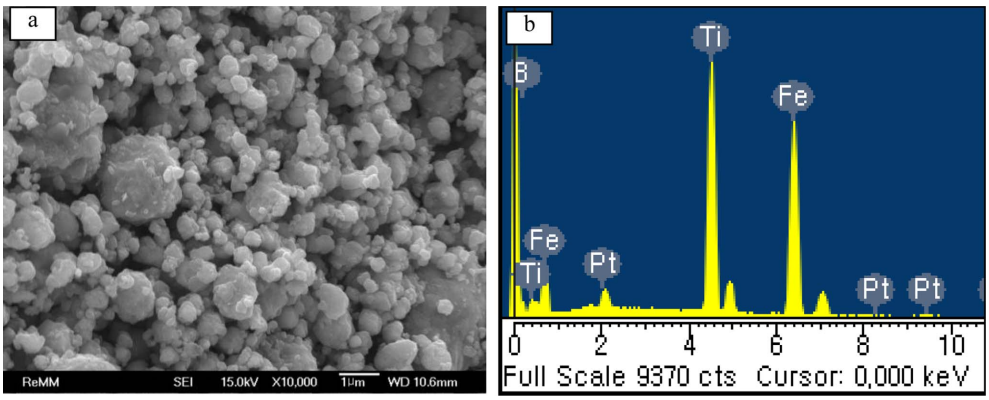

Fig. 6. FE-SEM image shows (a) morphology and (b) EDS result of Fe-TiB_2 composite powder after reaction synthesis at 1200°C for 5 hour.

These value indicates that TiB_2 is thermodynamically most favourable and the most stable phase. The reason for the formation of Fe_2B can be explained by reaction (3), when B in FeB particles reacts with Ti on surface to form TiB_2, and B content in FeB particle was depleted causing the transform of FeB to Fe_2B by the newly pure Fe on surface.

The morphology of Fe-TiB_2 composite powder after heat treatment at 1200°C for 5 hour is given in Fig. 6. It is hardly to identify TiB_2 particle on the surfaces but Fe, Ti and B peaks appearing in EDS spectra implies that the ultrafine TiB_2 particles in the Fe matrix.

Alternatively, TiB_2 particles can be identified using etching step to remove Fe matrix and to leave TiB_2 nanoparticles on the surface (Fig. 7(a)). The nanoscale TiB_2 particles form networks surrounding on the surface as shown in Fig. 7(b).

Fig. 8 shows cross-section images of powder particles after heat treatment and describes the evolution of composites microstructure after thermal reaction. Microstructure is composed of round-bright phase embedded in the dark phase (Fig. 8(a)). Comparing Fig. 8(a) with Fig. 3(c), it can be seen that the fine FeB particles in Fig. 3(c), particle size below 1mm, were disappeared in

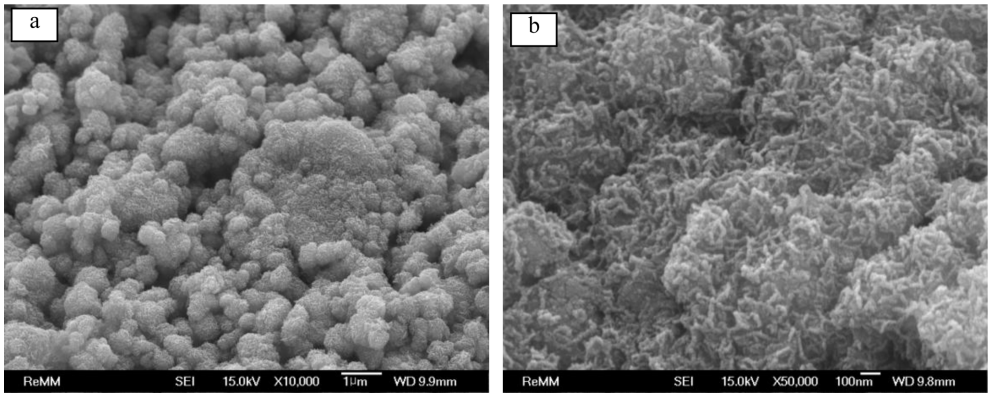

Fig. 7. FE-SEM image of Fe-TiB_2 composite powder after etching: (a) Low and (b) high magnification.

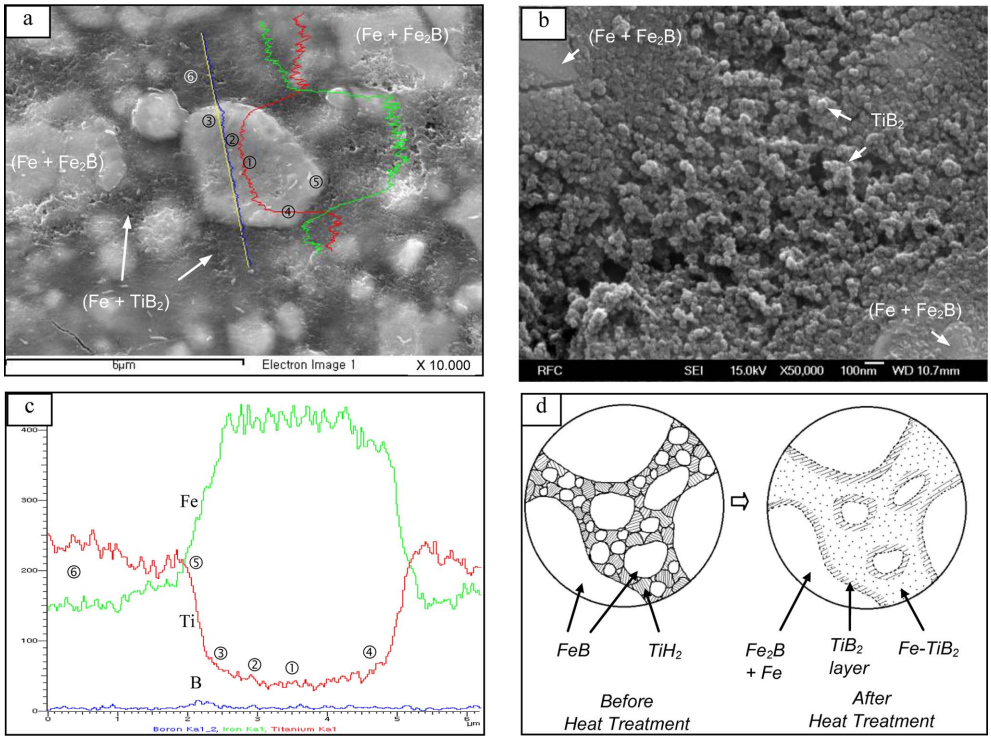

Fig. 8. FE-SEM image of microscopic cross-section of Fe-TiB_2 composite powder after (a) polishing and (b) etching. (c) Result of EDS line scan across the area marked in (a). In (d) the formation of microstructure is given schematically.

Table 2. Result of EDS composition analysis on cross-section surface marked in Fig. 8(a)

Points	Fe	Ti	Position	Phase composition
	Atomic (%)			
1	96.07	3.93	Centre	Fe_2B-Fe
2	95.62	4.38	Centre	
3	83.36	16.64	Layer	Fe_2B-Fe-TiB_2
4	83.79	16.21	Layer	
5	72.11	27.89	Boundary	Fe- TiB_2
6	46.86	53.14	Dark phase	Fe- TiB_2-Ti

microstructure of Fig. 8(a). It means that the fine FeB particles completely reacted with Ti to form TiB_2 particles in Fe matrix. Fig. 8(b) shows the dark phase surface after etching, which is composed of Fe and TiB_2. It is noteworthy that the TiB_2 particle is extremely fine, around 50 nm, in comparison with previous results reported by others. The received TiB_2 particle size was very coarse from several to tens micrometer [2, 4-8]. With coarse FeB particles, TiB_2 was formed firstly on the surface, gradually created network of TiB_2 particles surrounding Fe_2B core (Fig. 8(d)). This formation might prevent the further diffusion of boron to the matrix boundary and remained a large amount of Fe_2B in the powder after heat treatment.

Fig. 8(c) is result from EDS line scanning of bright phase on the Fig. 8(a), showing distribution of Fe, Ti and B. Fig. 8(d) shows the schematic figure on mechanism of phase formation after heat treatment. The concentration of Ti and B are higher at boundary (Point ⑤ in Fig. 8(c)) due to TiB_2 layer as mentioned above (Fig. 8(d)). The bright phase has Fe concentration much higher than that the dark phase, while Ti distribution is higher in the dark phase, as presented in the Table 2.

Table 2 shows composition of selected points analysed on microscopic cross-section surface of the composite. Most of Ti was concentrated in the dark phase, it is clearly that the dark phase is almost the Fe-TiB_2 composite, in which a small amount of Ti can be included that is hardly to detect within the resolution of X-ray diffraction. The bright phase was assigned for Fe_2B-Fe due to the highest Fe concentration in this phase.

4. Conclusions

Fe-TiB_2 composite powder was *in situ* synthesized from FeB and TiH_2 precursors by using high-energy mechanical milling and subsequent heat treatment process.

1) The FeB-TiH_2 powder mixture after mechanical milling is fine with agglomerates. The agglomerate was composed of fine TiH_2 embedded around FeB particles. The process did not generate new phases, but lowered temperature of TiH_2 dehydrogenation events.

2) DSC analysis confirms that TiH_2 dehydrogenation occurs above 500ºC for starting powder and 370ºC for milled powder mixtures, while TiB_2 formation is at higher temperature, above 910ºC.

3) A large amount of Fe_2B phase exists in final product after heat treatment. The TiB_2 particles create network surrounding the surface of coarse Fe-Fe_2B particles. Microstructure of the composite is characterized by the Fe-TiB_2 that was formed from fine FeB particles, embedded around the Fe-Fe_2B. Nanoscale TiB_2 particles were uniformly distributed in the Fe matrix with particle size around 50 nm.

Acknowledgements

This work was supported by the 2008 Research Fund of the University of Ulsan (2008-0116).

References

[1] H. O. Pierson: Handbook of Refractory Carbides and Nitrides, William Andrew Publishing/Noyes, 1996.
[2] C. C. Degnan and P. H. Shipway: Metall. Mater. Trans. A, **33** (2002) 2973.
[3] R. M. Aikin, Jr.: JOM, **49**(8) (1997) 35.
[4] B. S. Du, Z. D. Zou, X. H. Wang and S. Y. Qu: Mater. Lett., **62** (2008) 689.
[5] B. S. Du, Z. D. Zou, X. H. Wang and S. Y. Qu: Appl. Surf. Sci., **254** (2008) 6489 .
[6] M. Darabara, G. D. Papadimitriou and L. Bourithis: Surf. Coat. Technol., **201** (2006) 3518.
[7] Animesh Anal, T. K. Bandyopadhyay and K. Das: J. Mater. Process. Technol., **172** (2006) 70.
[8] O. K. Lepakova, L. G. Raskolenko and Y. M. Maksimov: Combust. Explos., **36**(5) (2000) 575.
[9] E. G. Avvakumov, A. R. Potkin and O. I. Samarin: Planetary mill. Author's certificate No. 975068, USSR, Patent Bulletin, No. 43 (1982).
[10] V. Bhosle, E.G. Baburaj, M. Miranova and K. Salama: Mater. Sci. Eng. A, **356** (2003) 190.
[11] NIST-JANAF Thermochemical Tables Fourth Edition

Part I, Al-Co, W.C. Malcolm, Jr.(Ed.), American Institute of Physics, (1998) 276.
[12] ibid, (1998) 539.
[13] ibid, (1998) 1341.
[14] J. C. Gachon, M. Notin and J. Hertz: Thermochim. Acta., **48** (1981) 155.